

Materials Research Express



PAPER

Study and analysis of the morphological, elemental and electrical properties of phosphorus doped monocrystalline silicon solar cell

RECEIVED

6 January 2019

REVISED


2 February 2019

ACCEPTED FOR PUBLICATION

14 February 2019

PUBLISHED

22 February 2019

S Biswas^{1,6}, M K Basher^{2,6}, M Khalid Hossain^{2,3,6} , M A R Akand², M T Rahman⁴, M R Ahmed¹, M A Matin⁵ and S Huque¹

¹ Institute of Energy, University of Dhaka, Dhaka 1000, Bangladesh

² Institute of Electronics, Atomic Energy Research Establishment, Bangladesh Atomic Energy Commission, Dhaka 1349, Bangladesh

³ Dept. of Advanced Energy Engineering Science, IGSES, Kyushu University, Fukuoka 816-8580, Japan

⁴ Dept. of MSE, University of Rajshahi, Rajshahi 6205, Bangladesh

⁵ Dept. of GCE, Bangladesh University of Engineering and Technology, Dhaka 1000, Bangladesh

⁶ Authors contributed equally to this work.

E-mail: khalid.baec@gmail.com

Keywords: sheet resistance, bulk concentration, conductivity, monocrystalline silicon solar cell, diffusion time

Abstract

In this study, the impact of diffusion time on monocrystalline silicon solar cell has been analysed morphologically, elementally, and electrically by adjusting diffusion time to establish optimized properties for high-efficiency. P-type raw wafers were prepared for diffusion following cleaning and wet etching operation. POCl₃ diffusion was done by varying diffusion time with a constant flow rate of process gases. The morphological and elemental studies were carried out with scanning electron microscope (SEM), and energy dispersive x-ray spectroscopy (EDX) respectively. Four-point probe test and Hall Effect measurement were used for studying the electrical characteristics (sheet resistance, resistivity, conductivity, and bulk concentration). From SEM result analysis, noticeable structural damages were found with the increase of doping time. Surface reflectance measurement (SRM) also supported the morphological distortion. Phosphorus, oxygen, silicon, and boron were traced by EDX analysis. The formation of phosphosilicate glass (PSG), as well as the depth of emitter, has been confirmed from the elemental analysis. The emitter length was varied from 2.5 μm to 9 μm . 5 min doped sample showed minimum surface deformation with maximum light absorbance. An acceptable sheet resistance with a compatible conductivity, mobility, and bulk concentration are also found for 5 min diffusion, which could potentially lead to high-efficient solar cell fabrication.

1. Introduction

Production of electric current from solar energy does not require fuel costs, and day by day it is becoming more affordable. Therefore, the accumulation of solar energy using solar cells has been expanding faster than other renewable sources since last few decades [1–8]. Among all the cells, monocrystalline silicon photovoltaic cells are the leading performer in harnessing solar incident. The overall efficiency largely depends on the quality of emitter layer of the conventional crystalline solar cell [8–12]. On the other hand, the POCl₃ diffusion significantly depends on the doping time, temperature, flow rate of the process gases i.e. N₂, O₂ etc [12–14]. Thus the impact of these parameters on (POCl₃) diffusion is important to analyse properly for the optimization of the morphological, elemental and electrical properties of the fabricated solar cells.

To increase the light absorbance as well as to improve the performance, surface roughness needs to be raised by texturization [15–18]. Treating the silicon wafer with process gases for a long time in a POCl₃ diffusion furnace at a high temperature would affect the textured surface which can lead to the decrease of the cell efficiency [19]. Moreover, the formation of a phosphosilicate glass (PSG) layer, a dopant source during the diffusion process, has displayed a distinct relationship with the quality of the emitter [12].

On the other side, sheet resistance identifies the quality of the n-type emitter [20]. The sheet resistance (ρ_{sh}) of the n-type incorporated with dopant impurities also determines the current density (J_{sc}), contact resistance properties and the quantum efficiency. A low sheet resistance (for instance $<60 \Omega/\square$) would result in lower short circuit current (I_{sc}) [21]. The low interfacial resistance between metals and the semiconductor is substantially dependent on higher doping density, which relies on the doping time [22–27]. Bulk doping level also significantly influences bulk recombination as well as the minority carrier lifetime. Raw wafers with low acceptor concentration (N_A) produce lower cell voltage and higher resistivity, whereas the higher density would result in a fall of I_{sc} and V_{oc} [21, 28]. Hence, the doping concentration needs to be optimized for the fabrication of the silicon cell [28]. Theoretical study and simulation of these parameters were done frequently rather than practical studies [29–31]. On this account, electrical characteristics of crystalline silicon photovoltaic cells are studied by varying the doping time on the current research. Moreover, the effect of longtime doping on the textured surface, and on the emitter is also assessed for the first time.

In this research, monocrystalline boron doped silicon wafers were fabricated using different doping time of phosphorus diffusion process. The SEM, EDX analysis has been conducted out for morphological and elemental studies to understand the impact of morphological changes on surface reflectance. Sheet resistance and bulk carrier density were measured with the help of a four-point probe and Hall Effect measuring system respectively. Klaassen's model [32] is used to determine the impact of doping time on the carrier mobility. An optimized doping time has been proposed on which all the properties can be optimized for the fabrication of high efficient solar cell.

2. Experimental

For the fabrication of solar cell, boron (B) doped Czochralski (Cz)—Monocrystalline Silicon wafers (ReneSola, China) have been taken which have a thickness of $180 \pm 20 \mu\text{m}$; a lifetime of $\geq 12 \mu\text{s}$; resistivity $1\text{--}3 \Omega\text{cm}$ and the dimension of $127 \times 127 \text{ mm}^2$. Five pseudo-squared samples were gone through the process named saw damage removal processing with the solution of NaOH and Di-water at 70° for 10 min. For roughening the surface and minimizing the reflectance, wet chemical etching was done with KOH solution, IPA (isopropanol) and Di-water for 20 min. To form the n-type emitter, all the samples were placed in the tube furnace (MRL PHOENIX, USA) for POCl_3 diffusion one after another for different doping time i.e. 5 min, 10 min, 15 min, 20 min, and 25 min respectively at 875°C temperature and in a constant flow of process gas (N_2 , O_2).

The effect of the doping time on the morphology of the textured wafers was observed using an SEM (Zeiss Evo 18, USA). After diffusion, the cross-sectional areas were also examined using FESEM (JSM-7600F, USA) to understand the height and the structural conditions of the produced pyramids due to texturization. Elemental analysis of the surface was done with two different beam acceleration voltages (5 kV and 20 kV), so that elements status both on the surface layer and the immediate layer under approximately $3.5 \mu\text{m}$ can be observed [33, 34]. The drive-in time (15 min) and surface passivation time (10 min) were constant for all of the samples so that only the impact of diffusion time can be observed accurately.

The effect of the structural changes and surface reflectance of the samples has been measured with the SRM system. Sheet resistance measurement was performed to study the doping quality as well as the electrical characteristics with the four-point probe measurement system (Keith Link, USA). Each test was repeated several times to ensure the accuracy. Hall Effect measurement was used to measure the carrier concentration of the doped wafers [35].

3. Results and discussion

3.1. Morphological analysis

The SEM images in figure 1 shows the morphology of the POCl_3 doped silicon wafers at different times. According to figure 1, it has been clearly observed that damages due to diffusion were considerable. Sample 1 (figure 1(a)) and sample 2 (figure 1(b)) have well-distributed pyramids with almost regular shape. When the diffusion time was increased to 15 min (figure 1(c)) the arrangement of pyramids became non-uniform as well as unoccupied spaces were found. In the case of sample 4 (figure 1(d)), though the pyramids were well-arranged, the height of the pyramids was declined. From the analysis of the cross-section view of the wafers (figure 2), it is clearly found that the height of the upright pyramids was decreasing with the increase of doping time. The average heights were found $4.12 \mu\text{m}$, $3.577 \mu\text{m}$, $2.988 \mu\text{m}$, $2.87 \mu\text{m}$, and $0.967 \mu\text{m}$ for the sample 1, sample 2, sample 3, sample 4 and sample 5 respectively, whereas before doping average height of textured sample was $4.3 \mu\text{m}$. The average height of the alkaline-based etching was found in the range of $2 \mu\text{m}$ to $8 \mu\text{m}$, which supports the previous findings [36].

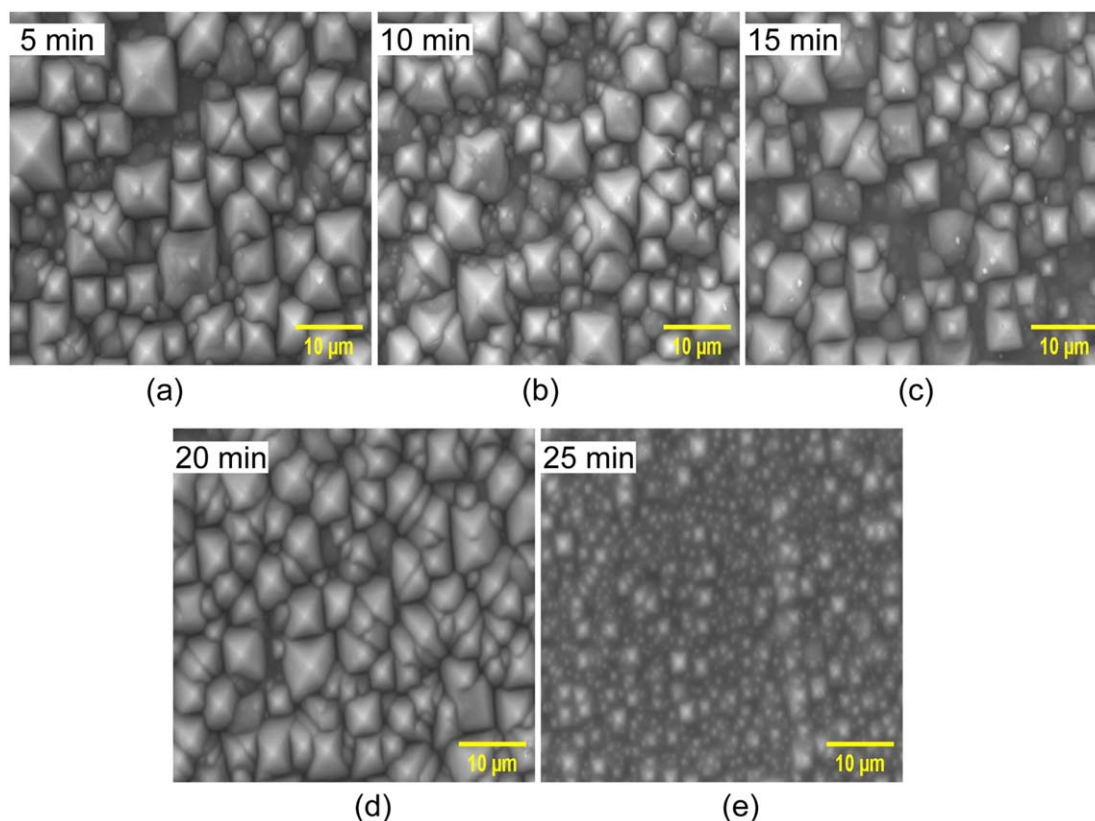


Figure 1. Morphological changes of the doped silicon wafers at different times: (a) 5 min (b) 10 min (c) 15 min (d) 20 min and (e) 25 min.

It is found that pyramidal shapes were damaged significantly when the samples were doped more than 15 min. The pyramids of 25 min doped sample (figure 1(e)) were demolished considerably which resulted in tiny sizes of the pyramids; thus significant deformation on the textured surface is observed due to increase of diffusion time. The impact of decreasing the height of pyramids lowers the percentage of reflectance of light from the surface of the sample. The result of surface reflectance showed that it had changed with the variation of diffusion time. Figure 3 depicts the rate of reflectance increases with the increase of diffusion time. The average reflectance of sample 1 (16.184%) was dropped by almost 63% compared to the raw wafer (43.71%), whereas the percentage changes only 12.83% in case of sample 5 (figure 4).

Therefore, it is observed that the percentage of reflectance is directly related to the height of the pyramids (figure 5). The average percentage of reflectance of visible light (400 nm to 900 nm) was found lowest when the average height of the pyramids became highest and vice versa [37].

A dark layer was also observed in cross-sectional SEM analysis (shown in figure 5) in the n-type region along with a very thin phosphosilicate glass (PSG) layer. This was confirmed with the help of EDX which is discussed in the next section. Jonas Krause *et al* also found a similar type of layer in a depth of approximately 10 μm in Al doped silicon [38].

According to the SEM analysis, the average height of sample 1 (5 min doped) was found 3.963 μm , and above the doping time 15 min the change of average height remains almost constant which was found between 8.9 to 9.1 μm (figure 6).

3.2. Elemental analysis

EDX analysis proves the presence of phosphorus, silicon, and oxygen atoms according to their proportion of mass (figure 7), which is higher in the top region. It is also identified that the atomic mass percentage of phosphorus and oxygen is significantly low whereas the amount of silicon becomes higher for the middle portion of the sample. This is pointing to the formation of the PSG ($\text{P}_2\text{O}_5\cdot\text{SiO}_2$) at the top, as it has more oxygen and silicon. The amount of oxygen is drastically dropped whereas there is still a significant percentage of the mass of phosphorus in the intermediate or the lower portion of the darker region. This confirms both the formation of PSG (at the surface) and the n-type emitter after that. The lighter portion has about 99% of silicon by atomic mass indicates the approximate ending of the emitter layer.

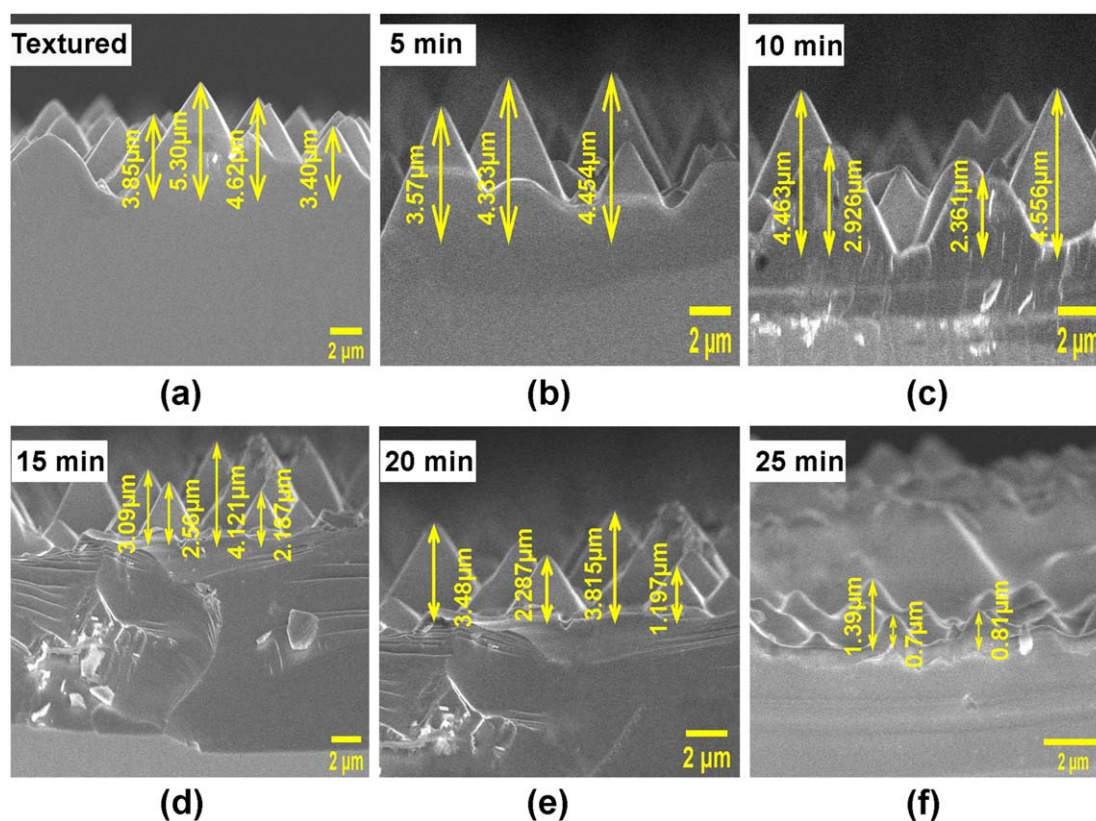


Figure 2. Cross-sectional view of SEM images of the wafers with different doping time: (a) textured before doping (b) 5 min (c) 10 min (d) 15 min (e) 20 min and (f) 25 min.

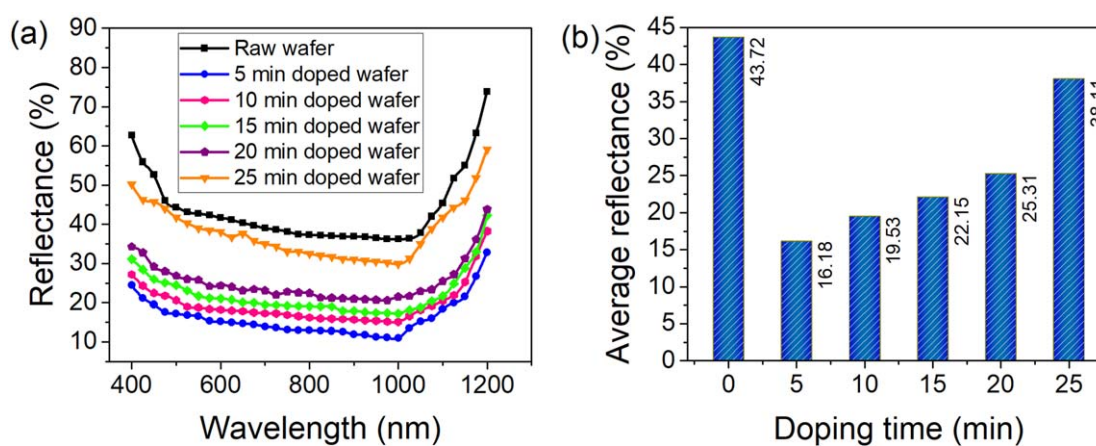
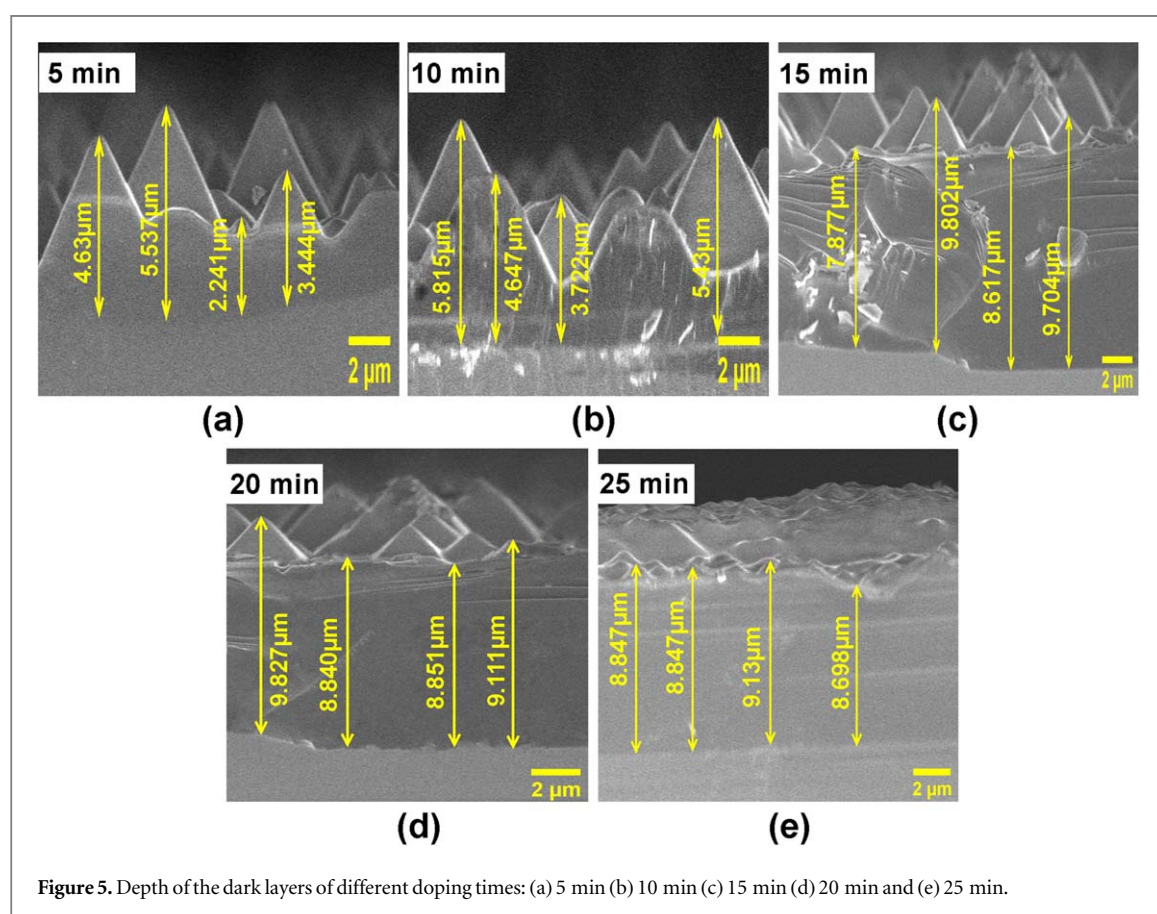
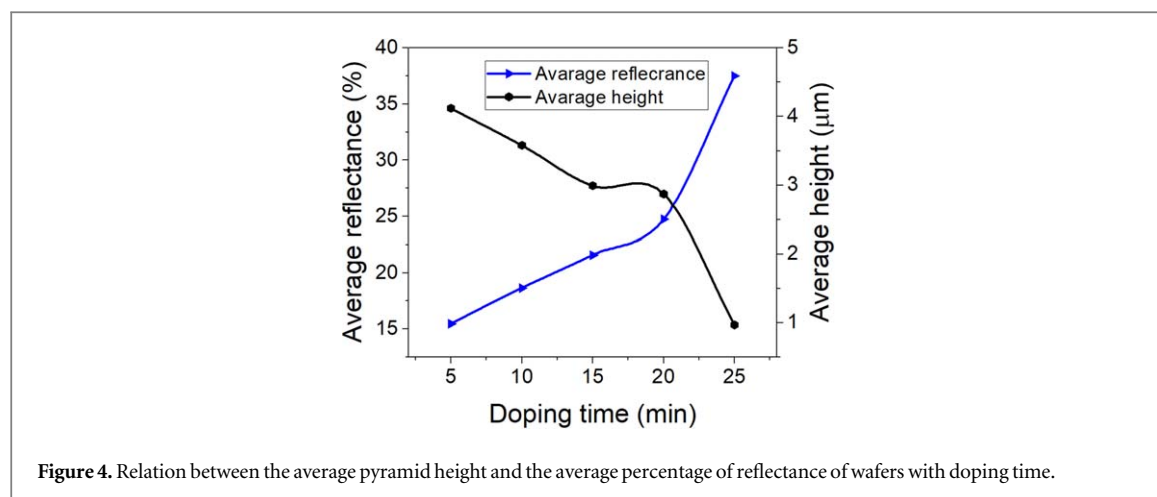


Figure 3. Optical analysis: (a) changes of percentage of reflectance of doped wafers with incident light wavelengths; (b) average surface reflectance varies with doping time.

The figure 8(a) represents the percentage of the atomic mass of the crucial elements found at 5 kV beam acceleration speed, which would penetrate only $0.30 \mu\text{m}$ of the surface [34]. The sample without doping had only a few percentages of boron ensure the p-type characteristics, whereas others certify the formation of the n-type emitter. When doping time was increased the amount of oxygen along with the phosphorus was getting high. This indicates the uplifting relation between time and deposition of phosphorus as well as oxygen which demonstrates the formation of PSG layers on the surface area.

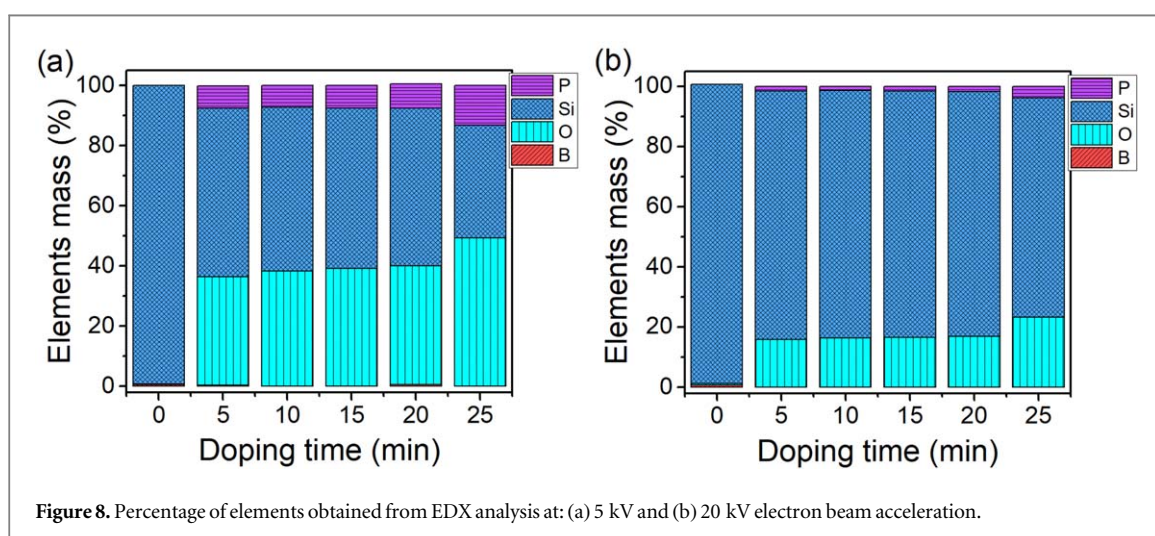
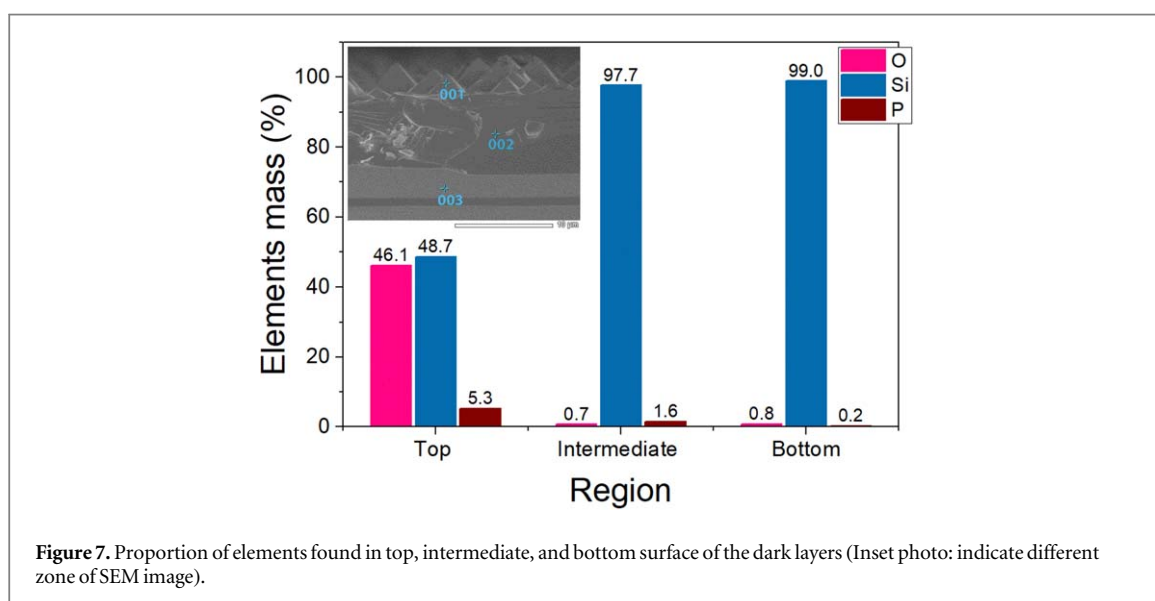
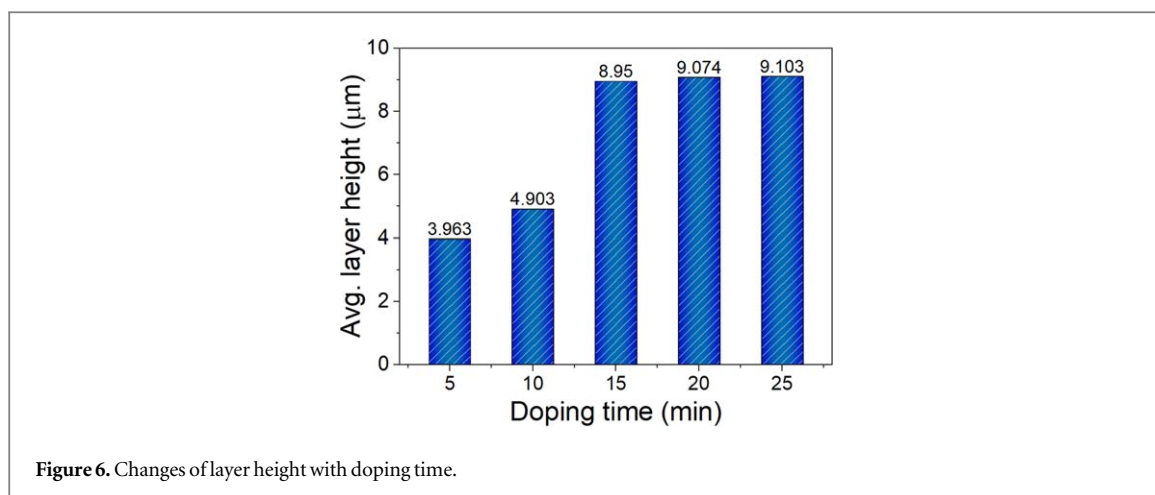
On the other hand, the amount of the doping element was decreasing at $3.5 \mu\text{m}$ depth [26] shown in figure 8(b). More solid silicon was found which was predicted as well. It is now clear from the SEM and the EDX analysis that, the length of the p-type differs for varying the doping time and after 20 min becomes almost fixed (approximately $9 \mu\text{m}$). From the comparison of the results obtained by 5 kV and 20 kV (figure 8) the amount of



phosphorus is increasing and also penetrate more depth when doping time increases. Moreover, the declining mass of oxygen clears the concept that the layer of PSG is very thin.

3.3. Electrical analysis

The sheet resistances (figure 9) were found 65.25, 55.38, 44.62, 39.53, 32.72, and 27.17 Ω/\square , with doping time of 5, 10, 15, 20, and 25 min respectively. A descending trend of sheet resistance was observed with the increment of doping concentration of phosphorus with the increase of diffusion time [39, 40]. The comparatively shallow low sheet resistance in traditional monocrystalline silicon cells is chosen to promote a low-resistance ohmic contact between the screen-printed metal and the emitter layer [41]. Very low sheet resistance causes the loss of blue response along with low short circuit current and low open circuit voltage [42]. However, the heavy doping increases carrier recombination in the emitter layer and the resistive power loss has a linear relationship with sheet resistance. Hence, to minimize high power loss the preferable sheet resistance is 60–100 Ω/\square [21, 43].



Nian Chen *et al* reported a regular three-bus-bar silicon solar cell where emitter sheet resistance was in the range of 70–90 Ω/\square [42]. Therefore, 5 min doping time gives the expectable sheet resistance.

The obtained sheet resistance (ρ_{sh}) was used to calculate the conductivity (σ) by following the equation given by Heaney *et al* [44] is tabulated in table 1.

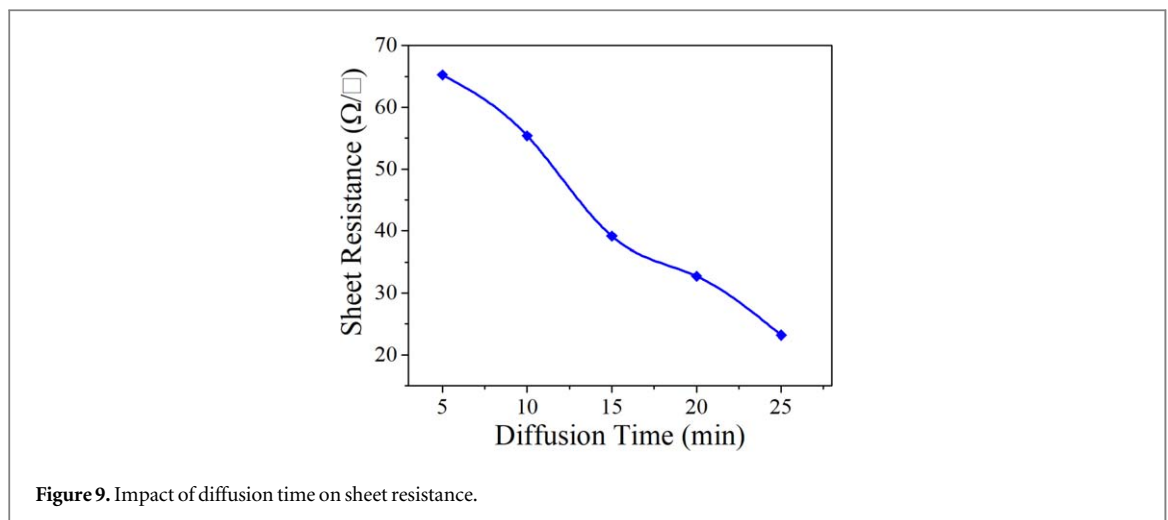


Figure 9. Impact of diffusion time on sheet resistance.

Table 1. Resistivity and conductivity of doped wafers.

Doping time (min)	Sheet resistance (Ω/\square)	Layer height (μm)	Resistivity (Ωcm)	Conductivity ($\Omega^{-1}\text{cm}^{-1}$)
5	65.25	3.96×10^{-6}	2.59×10^{-4}	3.87×10^3
10	55.38	4.09×10^{-6}	2.27×10^{-4}	4.41×10^3
15	39.14	8.95×10^{-6}	3.50×10^{-4}	2.85×10^3
20	32.72	9.07×10^{-6}	2.97×10^{-4}	3.37×10^3
25	23.17	9.10×10^{-6}	2.11×10^{-4}	4.74×10^3

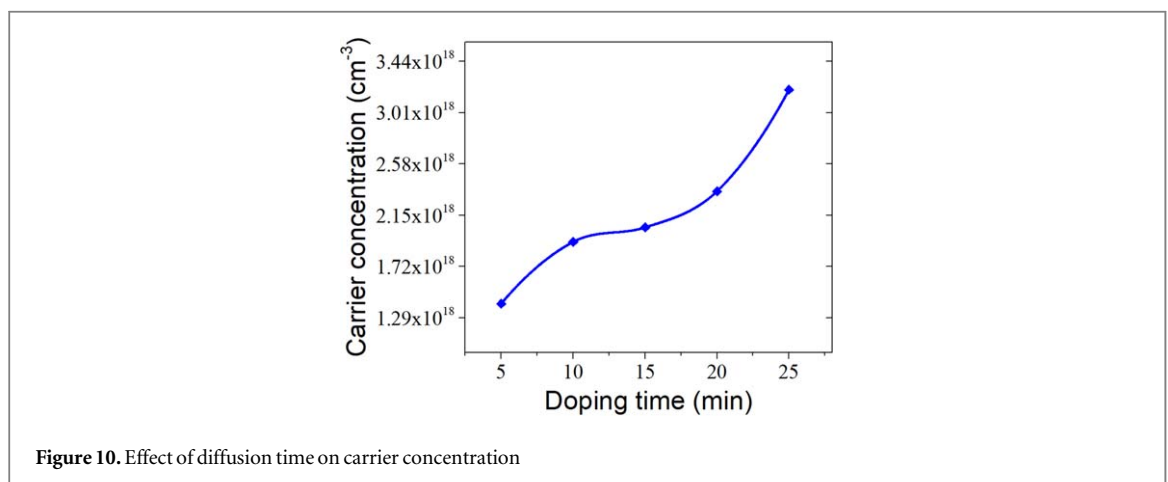


Figure 10. Effect of diffusion time on carrier concentration

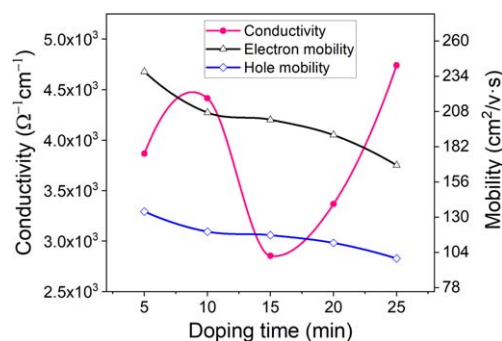
Figure 10 shows the surface concentration (N) of the wafers which changes between 1.41×10^{18} to 3.20×10^{18} (intermediate range) [20] with an increasing pattern. In this case, the highest concentration of the active phosphorus (P) was found due to 25min diffusion with considerably lower resistivity. Mousty *et al* also got similar type relationship between the resistivity and carrier density [45]. Doping of 10^{18}cm^{-3} is fairly suitable for solar cells as concentration $>10^{19}$ elevates band gap narrowing, Auger recombination as well as high surface recombination velocity [46].

The electron and hole mobility are found using Klaassen's model. In these case, the values of maximum and minimum mobility (μ_{max} , μ_{min}), reference concentration ($N_{\text{ref},1}$, $N_{\text{ref},2}$), fitting parameters (α_1 , α_2 , μ_1) for electron (phosphorus) and hole (boron) are given in table 2 [32, 47].

The conductivity was calculated with the assumed average emitter layers which were obtained from the elemental and cross-sectional view of SEM analysis. Figure 11 shows that the conductivity of the samples fluctuated randomly. This is because of the continuous increase of emitter depth and randomness of sheet resistivity. Both electron and hole mobility depend on the concentration of the dopant. In this case, both electron and hole mobility followed a steady downward trend with respect to doping time increment. The reason behind this phenomenon is the higher surface concentration (10^{18}cm^{-3}) of carrier density [32, 48]. The calculated electron mobility varied from $237\text{cm}^2\text{v}^{-1}\text{s}$ to $168\text{cm}^2\text{v}^{-1}\text{s}$ and the hole mobility varied from

Table 2. Model parameters for the majority electron mobility and majority hole mobility [32, 48].

Parameter	Phosphorus (P)	Boron (B)
μ_{\min} ($\text{cm}^2 \text{V}^{-1} \text{s}^{-1}$)	68.5	44.9
μ_{\max} ($\text{cm}^2 \text{V}^{-1} \text{s}^{-1}$)	1414	470.5
μ_1 ($\text{cm}^2 \text{V}^{-1} \text{s}^{-1}$)	56.1	29
$N_{\text{ref},1}$ (cm^{-3})	9.20×10^{16}	2.23×10^{17}
$N_{\text{ref},2}$ (cm^{-3})	3.41×10^{20}	6.10×10^{20}
α_1	0.711	0.719
α_2	1.98	2

**Figure 11.** Changes of conductivity and mobility with doping time.

134 $\text{cm}^2 \text{V}^{-1} \text{s}$ to 100 $\text{cm}^2 \text{V}^{-1} \text{s}$. Though higher concentration is obtained for 25 min diffusion, the other electrical parameters are not suitable for longer doping time. A low blue response, lower value of I_{sc} and V_{oc} can be obtained for sheet resistance below 60 Ω/\square [42]. Therefore, carrier concentration $1.41 \times 10^{18} \text{cm}^{-3}$ is a fair value for fabrication of silicon solar cells, which is achieved in 5 min doped sample. Also 5 min doping sample provide an acceptable sheet resistance, doping concentration, moderate conductivity as well as lower resistivity including higher mobility which indicates a better optimization can be achieved at 5 min diffusion.

4. Summary

In this study, the impact of phosphorus diffusion time has been analysed morphologically, elementally and electrically to establish an optimized doping time. The morphological study has proved structural damages due to increasing of the doping time. The formation of PSG as well as the emitter has been confirmed from the elemental analysis (EDX). Incorporating the SEM and EDX results, the emitter length is assumed which varied from 4 μm to 9 μm . The 5 min doped sample showed minimum surface deformation with maximum light absorbance. The surface reflectance measurement result proves that only 12.83% of reflectance reduced from the raw wafers for 25 min of diffusion, whereas 5 min doped sample has a reduction of reflectance of about 63% which indicated the impact due to structural distortion. The elemental analysis demonstrates the formation of PSG on the top layer of Si wafers. The height of the n-type region also became almost constant from 15 min of doping time, though the percentage of the mass of deposited phosphorus was increasing. Considering the electrical properties, sheet resistance was decreasing whereas the bulk concentration was increasing due to greater doping time. In this case, the 5 min doped sample gave carrier concentration of $1.41 \times 10^{18} \text{cm}^{-3}$ with a sheet resistance of 65.25 Ω/\square . The resistivity varied from 2.58×10^{-4} to $3.5 \times 10^{-4} \Omega\text{cm}$ and conductivity varied from approximately 2854 to 4741 $\Omega^{-1} \text{cm}^{-1}$. 25 min doping sample showed lower resistivity, higher carrier mobility, and better conductivity. The possible reason is the lower sheet resistivity and higher carrier concentration, which may cause low current density as well as higher contact resistance. Considering all, 5 min doped solar cell having well-shaped pyramids, has been optimized with the lowest amount of reflectance of light (16.18%), better sheet resistance, carrier concentration, a compatible conductivity ($3867.19 \Omega^{-1} \text{cm}^{-1}$), electron-hole mobility and noticeably lower resistivity ($2.58 \times 10^{-4} \Omega\text{cm}$), which facilitate the fabrication of high efficient monocrystalline silicon solar cells.

Acknowledgments

The authors are grateful to Institute of Electronics of Bangladesh Atomic Energy Commission (BAEC) to support this work, Dept. of GCE, Bangladesh University of Engineering and Technology (BUET) for SEM and EDX analysis, and IFRD, Bangladesh Council of Scientific and Industrial Research (BCSIR) for Hall Effect Measurement.

ORCID iDs

M Khalid Hossain  <https://orcid.org/0000-0003-4595-6367>

References

- [1] Moriarty P and Honnery D 2012 What is the global potential for renewable energy? *Renew. Sustain. Energy Rev.* **16** 244–52
- [2] Kalita P, Dewan A and Borah S 2016 A review on recent developments in solar distillation units *Sadhana* **41** 203–23
- [3] Peter L M 2011 Towards sustainable photovoltaics: the search for new materials *Philos. Trans. R. Soc. A Math. Phys. Eng. Sci.* **369** 1840–56
- [4] M S, Lee Y, Ju M, Balaji N, Kumar S and Yi J 2012 Fabrication of Crystalline Silicon Solar Cell with Emitter Diffusion, SiNx Surface Passivation and Screen Printing of Electrode *Photodiodes—From Fundamentals to Applications* (London, United Kingdom: InTech) 105–32
- [5] Basher M K, Khalid Hossain M, Afaz R, Tayyaba S, Akand M A R, Rahman M T and Eman N M 2018 Study and investigation of phosphorus doping time on emitter region for contact resistance optimization of monocrystalline silicon solar cell *Results Phys.* **10** 205–11
- [6] Hossain M K, Mortuza A A, Sen S K, Basher M K, Ashraf M W, Tayyaba S, Mia M N H and Uddin M J 2018 A comparative study on the influence of pure anatase and degussa-P25 TiO₂ nanomaterials on the structural and optical properties of dye sensitized solar cell (DSSC) photoanode *Optik (Stuttg.)* **171** 507–16
- [7] Hossain M K, Pervaz M F, Mia M N H, Mortuza A A, Rahaman M S, Karim M R, Islam J M M, Ahmed F and Khan M A 2017 Effect of dye extracting solvents and sensitization time on photovoltaic performance of natural dye sensitized solar cells *Results Phys.* **7** 1516–23
- [8] Wang Q, Pan C, Chen K, Zou S, Shen M and Su X 2017 Efficient nanostructured quasi-single crystalline silicon solar cells by metal-catalyzed chemical etching *Sol. Energy Mater. Sol. Cells* **164** 40–6
- [9] Hu S M 1988 Effect of process parameters on stress development in two-dimensional oxidation *J. Appl. Phys.* **64** 323–30
- [10] Kobor D, Ndioukane R, Palais O, Touré M, Diallo A K, Fall N C Y and Biagui M 2015 Simple method for phosphorus diffusion on (100) oriented P-type silicon using new phosphorus gel as dopant *Appl. Phys. Res.* **7** 49–57
- [11] Ghembaza H, Zerga A, Saïm R and Pasquinelli M 2018 Optimization of phosphorus emitter formation from POCl₃ diffusion for p-type silicon solar cells processing *Silicon* **10** 377–86
- [12] Dastgheib-Shirazi A, Steyer M, Micard G, Wagner H, Altermatt P P and Hahn G 2013 Relationships between diffusion parameters and phosphorus precipitation during the POCl₃ diffusion process *Energy Procedia* **38** 254–62
- [13] Murukesan K, Kumbhar S, Kapoor A K, Dhaul A, Saravanan S, Pinto R and Arora B M 2014 POCl₃ diffusion process optimization for the formation of emitters in the crystalline silicon solar cells *2014 IEEE 40th Photovoltaic Specialist Conf. (PVSC) (IEEE)* pp 3011–3
- [14] Mandelkorn J, McAfee C, Kesperis J, Schwartz L and Pharo W 1962 Fabrication and characteristics of phosphorous-diffused silicon solar cells *J. Electrochem. Soc.* **109** 313
- [15] Bressers P M M C 1996 Surface morphology of p-type (100) silicon etched in aqueous alkaline solution *J. Electrochem. Soc.* **143** 1744
- [16] Hashmi G, Hasanuzzaman M, Basher M K, Hoq M and Rahman M H 2018 Texturization of as-cut p-type monocrystalline silicon wafer using different wet chemical solutions *Appl. Phys. A* **124** 415
- [17] Basher M K, Hossain M K, Uddin M J, Akand M A R and Shorowordi K M 2018 Effect of pyramidal texturization on the optical surface reflectance of monocrystalline photovoltaic silicon wafers *Optik (Stuttg.)* **172** 801–11
- [18] Basher M K, Hossain M K and Akand M A R 2019 Effect of surface texturization on minority carrier lifetime and photovoltaic performance of monocrystalline silicon solar cell *Optik (Stuttg.)* **176** 93–101
- [19] Kumar D, Saravanan S and Suratkar P 2012 Effect of oxygen ambient during phosphorous diffusion on silicon solar cell *J. Renew. Sustain. Energy* **4** 033105
- [20] Jia H, Luo L, Jiang Y, Xu Z, Ren X and Zhang C 2014 Diffusion process for efficiency improvement with high sheet resistance on traditional production lines of solar cell *Sci. China Technol. Sci.* **57** 962–7
- [21] Panek P 2016 The Influence of the base material parameters on quantum and photoconversion efficiency of the Si solar cells *Arch. Metall. Mater.* **61** 1889–94
- [22] Meier D L and Schroder D K 1984 Contact resistance: its measurement and relative importance to power loss in a solar cell *IEEE Trans. Electron Devices* **31** 647–53
- [23] Yang Y, Seyedmohammadi S, Kumar U, Gnizak D, Graddy E D and Shaikh A 2011 Screen printable silver paste for silicon solar cells with high sheet resistance emitters *Energy Procedia* **8** 607–13
- [24] Hossain M I, Qarony W, Hossain M K, Debnath M K, Uddin M J and Tsang Y H 2017 Effect of back reflectors on photon absorption in thin-film amorphous silicon solar cells *Appl. Nanosci.* **7** 489–97
- [25] Vinod P N 2005 Specific contact resistance of the porous silicon and silver metal ohmic contact structure *Semicond. Sci. Technol.* **20** 966–71
- [26] Vinod P N 2011 Specific contact resistance measurements of the screen-printed Ag thick film contacts in the silicon solar cells by three-point probe methodology and TLM method *J. Mater. Sci., Mater. Electron.* **22** 1248–57
- [27] Qarony W, Hossain M I, Hossain M K, Uddin M J, Haque A, Saad A R and Tsang Y H 2017 Efficient amorphous silicon solar cells: characterization, optimization, and optical loss analysis *Results Phys.* **7** 4287–93
- [28] Brown D J and Shannon C 2000 Uniqueness, stability, and comparative statics in rationalizable walrasian markets *Econometrica* **68** 1529–39
- [29] McCranie K D, Faulkner M, French D, Daddis G A, Gow J and Long A 2011 Book reviews *J. Strateg. Stud.* **34** 281–93

- [30] Wagner H, Dastgheib-Shirazi A, Chen R, Dunham S T, Kessler M and Altermatt P P 2011 Improving the predictive power of modeling the emitter diffusion by fully including the phosphosilicate glass (PSG) layer *2011 37th IEEE Photovoltaic Specialists Conference (IEEE) (Seattle, WA, USA) (IEEE)* pp 002957–62
- [31] García-Tabarés E, Martín D, García I and Rey-Stolle I 2013 Understanding phosphorus diffusion into silicon in a MOVPE environment for III–V on silicon solar cells *Sol. Energy Mater. Sol. Cells* **116** 61–7
- [32] Klaassen D B M 1992 A unified mobility model for device simulation—I. Model equations and concentration dependence *Solid. State. Electron.* **35** 953–9
- [33] Cox G A 1985 Fundamentals of energy dispersive x-ray analysis *Phys. Bull.* **36** 349
- [34] Lee S, Younan H, Siping Z and Zhiqiang M 2006 Studies on electron penetration versus beam acceleration voltage in energy-dispersive x-ray microanalysis *2006 IEEE Int. Conf. on Semiconductor Electronics (IEEE) (Kuala Lumpur, Malaysia) (IEEE)* pp 610–3
- [35] Sequeira C A C and Santos D M F 2007 Four-point probe electrical measurements on p–n–p InP structures *Brazilian J. Phys.* **37** 147–55
- [36] Han Y, Yu X, Wang D and Yang D 2013 Formation of various pyramidal structures on monocrystalline silicon surface and their influence on the solar cells *J. Nanomater.* **2013** 1–5
- [37] Cho C, Kong D, Oh J-H, Kim B, Lee B and Lee J 2014 Surface texturing method for silicon solar cell using reactive ion etching with metal mesh *Phys. Status Solidi* **211** 1844–9
- [38] Krause J, Woehl D B R and Biro D 2010 Analysis of local Al-P+ -layers for solar cells processed by small screen-printed structures *25th European Photovoltaic Solar Energy Conf. and Exhibition (Valencia, Spain)* pp 1899–904
- [39] Shen L, Liang Z C, Liu C F, Long T J and Wang D L 2014 Optimization of oxidation processes to improve crystalline silicon solar cell emitters *AIP Adv.* **4** 027127
- [40] Li H, Kim K, Hallam B, Hoex B, Wenham S and Abbott M 2017 POCl_3 diffusion for industrial Si solar cell emitter formation *Front. Energy* **11** 42–51
- [41] Cuevas A and Russell D A 2000 Co-optimisation of the emitter region and the metal grid of silicon solar cells *Prog. Photovoltaics Res. Appl.* **8** 603–16
- [42] Chen N, Tate K and Ebong A 2015 Generalized analysis of the impact of emitter sheet resistance on silicon solar cell performance *Jpn. J. Appl. Phys.* **54** 08KD20
- [43] Kulushich G, Bazer-Bachi B, Takahashi T, Iida H, Zapf-Gottwick R and Werner J H 2012 Contact formation on $100\omega/\text{sq}$ emitter by screen printed silver paste *Energy Procedia* **27** 485–90
- [44] Heaney M B 2003 Electrical Conductivity and Resistivity *Electrical Measurement, Signal Processing, and Displays* ed J G Webster (Washington DC, USA : CRC Press) pp 1–14
- [45] Masetti G, Severi M and Solmi S 1983 Modeling of carrier mobility against carrier concentration in arsenic-, phosphorus-, and boron-doped silicon *IEEE Trans. Electron Devices* **30** 764–9
- [46] Schindler F, Schubert M C, Kimmerle A, Broisch J, Rein S, Kwopil W and Warta W 2012 Modeling majority carrier mobility in compensated crystalline silicon for solar cells *Sol. Energy Mater. Sol. Cells* **106** 31–6
- [47] Mousty F, Ostojia P and Passari L 1974 Relationship between resistivity and phosphorus concentration in silicon *J. Appl. Phys.* **45** 4576–80
- [48] Upadhyaya A. D., Yelundur V and Rohatgi A 2006 High efficiency mono-crystalline solar cells with simple manufacturable technology *University Center of Excellence for Photovoltaics Conference Papers* 136 (Atlanta, GA, USA: Georgia Institute of Technology) 23–42